https://doi.org/10.48048/tis.2022.4611

Adsorption Characteristics of Thioflavin T on Activated Carbon from Oil Extracted *Elaeocarpus hygrophilus Kruz* Seeds

Chakkrit Umpuch[*], Konthong Jaroennit, Prapachuen Thummaporn, Rattiyaporn Chaithongsri and Channarong Puchongkawarin

Department of Chemical Engineering, Ubon Ratchathani University, Ubon Ratchathani 34190, Thailand

([*]Corresponding author's e-mail: chakkrit.u@ubu.ac.th)

Received: 16 May 2021, Revised: 27 June 2021, Accepted: 4 July 2021

Abstract

The adsorption of Thioflavin T (TT) dyes, cationic dyes, from aqueous solution using activated carbon (AC) from oil extracted *Elaeocarpus hygrophilus Kurz* seeds was studied in this work. The precursor, water olive seed, was ground for oil extraction by hexane, and then carbonized at 450 °C. The char and KOH were mixed at a mass ratio of 1: 3 and then activated at 780 °C. The carbonization and activation were done under a nitrogen atmosphere. The investigation was divided into 3 sections. The AC was firstly characterized by various techniques such as N_2 adsorption-desorption isotherm, FTIR, SEM and EDS. The batch adsorption tests were secondly conducted to study the effects of process parameters such as initial pH, contact time, initial dye concentration, and temperature on the performance of the adsorption. The highest dye uptake of 57.34 mg/g was observed under a certain condition: pH of 8.0, contact time of 60 min, initial dye concentration of 250 mg/L, and temperature of 60 °C. Finally, the experimental data were fitted to the adsorption models. The experimental data followed the pseudo-second-order reaction model and Langmuir and Freundlich isotherm equations. The AC from oil extracted *Elaeocarpus hygrophilus Kurz* seeds is an effective adsorbent for TT dye removal from wastewater.

Keywords: Thioflavin T, Activated carbon, *Elaeocarpus hygrophilus Kurz*, Adsorption, Wastewater

Introduction

Effluents discharged from many household-scale textile industries in the rural area of north-eastern Thailand are usually contaminated with chemical synthetic dyes. The synthetic dyes are preferentially used over the natural dyes because they are cheap and easy to find in the local area. In addition, their colour is bright and long-lasting [1]. The textile products such as cotton and silk weave are mostly coloured by these dyestuffs. Thioflavin T (TT) is a synthetic dye widely used to colour woven products such as silk, cotton, Niron, and acetate fiber [2]. The dye is highly dissolved in water and about half of the dye quantity is left in the water body after the dyeing process. High-level contamination of the dye in the nature causes negative impacts on the environment such as increasing chemical and biological oxygen demand (COD and BOD), entering the food chain, inhibiting the plant growth, impairing photosynthesis, and providing recalcitrance as well as bioaccumulation [3]. It is toxic to aquatic life with long lasting effects e.g. mutagenicity and carcinogenicity [5]. Also, it causes fatality or may produce serious damage to the health of the individual when exposed to the human body [6]. According to the environmental regulation in Thailand, the ADMI (American Dye Manufacturers Institute) colour scale is used as an indicator of water quality to measure the colour of wastewater. Therefore, it is required to remove the TT dye from the effluent so that its colour will be less than 300 ADMI before being discharge into the water body [7].

Dyes in wastewater can be removed by various methods categorized into 3 approaches: Physical, chemical and biological approaches. Physical methods include reverse osmosis, sedimentation, coagulation-flocculation, magnetic nanoparticle and adsorption [8]. Electrochemical oxidation, ion exchange, advanced oxidation by Fenton reagent, ozonation, photo-catalytic degradation by irradiation and electrocoagulation are some examples of chemical techniques [9]. Biological approaches include bacterial degradation, aerobic and anaerobic degradation, degradation using algal and fungal biodegradation [10]. Among these methods, adsorption is an efficient technique and has been widely

applied for dye removal from the effluent because of its low cost, high efficiency and easy operation & design. It is the binding of molecules and ions on the surface of the adsorbent by physical and chemical forces. Various materials such as activated carbon (AC) [11-13], mineral clay [14], green alga *Caulerpa scalpelliformis* [15], reed [16] and mineral stone [17] etc., are used as adsorbents for TT dye removal and found in the literatures. The adsorption of TT dyes on the AC from Ha Bac, kaolin, *Caulerpa* species, reed and *Moroccan Stevensite* was previously studied and the maximum adsorption capacities of these adsorbents were reportedly equal to 769.23, 2.174, 27, 140 and 454.3 mg/g, respectively. It is clearly found that dye uptake on the AC is significantly higher than other adsorbents so it is widely used as an adsorbent for TT dye removal [11].

AC is a carbonaceous material which has a porous structure with large surface area. It can be prepared from different raw materials with high carbon contents and small amount of inorganic. The commercial AC is typically expensive due to high cost of raw materials. An alternative way to reduce the cost is the use of cheap and widely available materials. Raw materials of the AC are generally residues from agriculture and forestry or biomass residue wastes e.g. rich hulls, walnut & hazelnut shells, hard shells of apricot stones and almond etc. These materials are mostly hard and woody [18]. One of the potential precursor for preparation of the AC is *Elaeocarpus hygrophilus Kurz* or "water olive" because its seed has a hard and woody shell. It is a tropical plant, an evergreen shrub or small tree, growing from 3 - 13 m tall [19]. It is tremendously found in the north-eastern part of Thailand, which is considered as a tropical region, especially the waterfront area. The fruit is available for half a year (between June to November). The seed is left as natural solid waste so it is priceless and largely available.

To our knowledge, there has not been any research conducted on the preparation of AC from the *Elaeocarpus hygrophilus Kurz* seed. Also, many studies have focused on preparing the AC from available raw materials without further pretreatment [20-22]. In this work, the preparation of the AC from the *Elaeocarpus hygrophilus Kurz* seed was focused with additional pretreatment by the solvent extraction technique to remove oil [23] before passing through the carbonization and activated processes. This could expectedly increase in the carbon content of the derived AC, providing more adsorption sites to the adsorbent. The characteristics of the derived AC was then investigated to reveal the transformation of the precursor into the carbon adsorbent such as N_2 adsorption-desorption isotherm at 77 K, FTIR, SEM and EDS [24,25]. In addition, the batch adsorption experiments were carried out to investigate the effects of the process parameters on the performance of the adsorption. The experimental data were then fitted to the well-established kinetic adsorption models and adsorption isotherm models.

Materials and methods

Dye and chemicals

TT ($C_{17}H_{19}ClN_2S$) with a molecular weight of 318.86 g/mol and hexane with a molecular weight of 86.18 g/mol were purchased from SIGMA-Aldrich (product no. T3516). TT is also known as basic yellow 1 and its structure is shown in **Figure 1**, which is modified from the product information sheet of the supplier .All chemicals were used as received without any further purification.

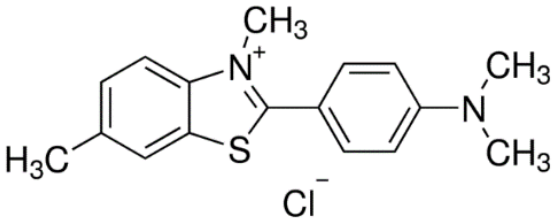

Figure 1 Chemical structure of the TT dye.

Preparation of AC

The *Elaeocarpus hygrophilus Kurz* seeds were collected from a local market in Ubon Ratchathani province, Thailand. The percentage of fixed carbon and other related parameters were analyzed by the procedure of the ASTM D3174-12 [26]. **Table 1** shows the properties of the *Elaeocarpus hygrophilus Kurz* seed. It was found that the seed contained the high carbon content or had a fixed carbon of 48.22 %. The high carbon content materials can provide a high yield of the AC.

Table 1 Average moisture, volatile matter, ash, and carbon contents of the *Elaeocarpus hygrophilus Kurz* seed.

Parameter	Value
Moisture content, %	11.98
Volatile matter, %	26.58
Ash content, %	13.22
Fixed carbon, %	48.22

The *Elaeocarpus hygrophilus Kurz* seed was washed 3 times by distilled water, oven-dried at 105 °C until its weight remained constant. It is then ground for oil extraction by soaking in the hexane solvent overnight. The oil free material was dried again in the oven at 105 °C. Later, the dried material was carbonized at 450 °C for 1 h. The product which is called 'char' was cooled by leaving it in the furnace. The char was further activated by mixing with KOH at a mass ratio (char/KOH) of 1: 3 and then carbonized again at 780 °C for 1 h. Carbonization was done under a nitrogen atmosphere. The naturally cooled product called "activated carbon" or AC was washed 3 times by 20 % v/v HCl to remove the remained KOH and washed many times by distilled water until the pH of the rinse water was equal to that of the distilled water. The carbon was ground and sieved through a 100-mesh sieve. The AC was stored in a desiccator for further modification.

Characterizations

The AC was characterized by various techniques such as specific surface area, pore size, and total pore volume evaluated from the N_2 adsorption-desorption isotherm using the BET method, BJH method, and N_2 adsorption volume at P/P_0 of 0.99, respectively. The chemical characterization of the AC was measured by the EDS (Energy-dispersive X-ray spectroscopy). Morphology of the adsorbent was studied from SEM (Scanning electron microscope) images. Possible active functional groups on the adsorbent were determined by the FTIR (Fourier Transform Infrared Spectrophotometer).

Batch adsorption tests

The batch adsorption tests were done as functions of initial pH, contact time, initial dye concentration, and temperature. The adsorbent dosage of 0.1 g was fixed throughout the whole experiments. Firstly, the effect of contact time was studied. Several Erlenmeyer flasks containing 100 mL of 150 mg/L dye solutions were prepared. The initial pH of solutions was adjusted to 4.0. For each flask, 0.1 g of the adsorbent was added to the dye solution and then shaken at a controlled temperature of 25 °C. The samples were measured at time intervals of 10, 20, 30, 40, 50, 60, 120, 180 and 250 min. The adsorbent was removed from the suspension by vacuum filtration and the filtrate was subjected to the UV Vis Spectrophotometer for measuring the absorbance at a maximum wavelength (λ_{max}) of 446 nm. The absorbance was then converted to the dye concentration remained in the liquid phase by the calibration curve (a plot of absorbance vs. dye concentration).

Secondly, the influence of initial pH was investigated. Another set of Erlenmeyer flasks containing 100 mL of 150 mg/L dye solutions was prepared. The different pH from 2.0 to 10.0 of the dye solutions was adjusted by adding 0.1M NaOH and/or 0.1M HCl. For each flask, 0.1 g of the adsorbent was added into the dye solution and then shaken at a controlled temperature of 25 °C for 24 h. The final dye concentration was evaluated in the same manner as in the first experiment. Thirdly, a set of Erlenmeyer flasks which contained 100 mL of 50 - 300 mg/L dye solutions was prepared to study the effect of initial dye concentration. The stock solution with the dye concentration of 1,000 mg/L was prepared by mixing 1 g of the dye with 500 mL of distilled water in a beaker, then poured in the 1,000 mL volumetric flask and filled up with another 500 mL distilled water. The dye solutions with various dye concentrations were prepared by the dilution method. Different quantities of the stock solution including 5, 10, 15, 20, and 25 mL were pipetted into a group of 100 mL volumetric flasks and then filled up with distilled water until the liquid volume in the flasks reached 100 mL. Thus, the dye solutions with different concentrations ranging from 50 to 250 mg/L were obtained, respectively. The initial pH of the solutions was adjusted to 4.0. The procedure was similar to the previous experiments. The effect of temperature on the adsorption was finally conducted. The batch test was carried out in the same manner as in the first experiment but the pH was fixed at 4.0 and the temperature was varied between 45 and 60 °C.

Results and discussion

Characteristics of the adsorbent

The N_2 adsorption-desorption isotherm of the AC at 77 K was analyzed. It was found that the adsorption isotherm followed Type I behavior classified by IUPAC. Normally, the Type I isotherm is characteristic for the microporous materials [27]. It is well documented [28] that the AC is a microporous material. The physical properties of the AC are given in **Table 2**. The specific surface area of the adsorbent analysed by the BET method was 29.97 m^2/g. The total pore volume analysed by t-plot was 0.03 cm^3/g. The average pore size was 1.60 nm considered as a microporous material (pore size is less than 2.0 nm).

Table 2 Physical properties of the AC.

Characteristic parameter	Value	Unit
BET specific surface area	29.97	m^2/g
Total pore volume	0.03	cm^3/g
Average pore size	1.60	nm

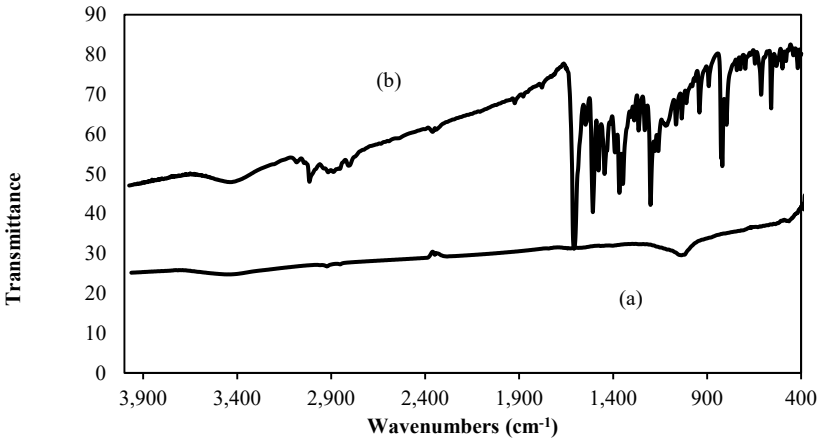

Figure 2 FT-IR analysis of (a) AC and (b) TT.

IR spectra of the AC are illustrated in **Figure 2(a)**. The vibration bands of O-H stretching (Hydroxyl, carboxylic and phenolic groups) at 3,467 cm^{-1}, C-H stretching (Alkane) at 2,895 cm^{-1}, C-H stretching (CH_2-CO-group) at 2,372 cm^{-1}, C = O stretching (Carboxylic groups) at 1,718 cm^{-1}, C-O stretching (Carboxylic groups) at 1,348 cm^{-1} and O-H bending (Carboxylic groups) at 1,018 cm^{-1} were observed [29-31]. The spectra of the TT dye are presented in **Figure 2(b)**. The O-H stretch vibrations of water impurities at 3,410 cm^{-1} and C-H (Alkane) stretch vibrations at 2,910 cm^{-1} were detected. The strong bands were also found at 1,610 and 1,510 cm^{-1} associated with the benzene ring skeletal C = C stretching vibrations, whereas another band associated with the bending vibrations of the C-H bonds of the aromatic ring was found at the 670-900 cm^{-1} region. There was a tertiary amine C = N stretch vibration band at 1,208 cm^{-1} [32,33]. The interactions between the TT and the AC involve van der Waals forces and the electrostatic attraction. The van der Waals forces are the interactions between the carbon atoms and other molecules [34]. The electrostatic attraction is the interactions between anionic functional groups of the AC such as carboxylic acid and hydroxyl groups and the cationic functional groups of the TT dye such amine group. It reveals that the surface of the AC contains both hydrophilic parts of the functional groups with negative charges and the hydrophobic parts of the carbon.

The elemental compositions presented in the EDS spectra of the ACs which were made from the oil extracted and non-oil extracted water olive seeds are depicted in **Figures 3(a)** and **3(b)**, respectively. Based on the EDS results, it could be observed that the major chemical element of the ACs was carbon. The AC made from the oil extracted water olive seed showed the slightly higher carbon content. Both ACs qualified the standards of the AC by SNI No.06-3730-1995 with a minimum carbon of 65 %. The result followed the percentage of the fixed carbon as presented in **Table 1**.

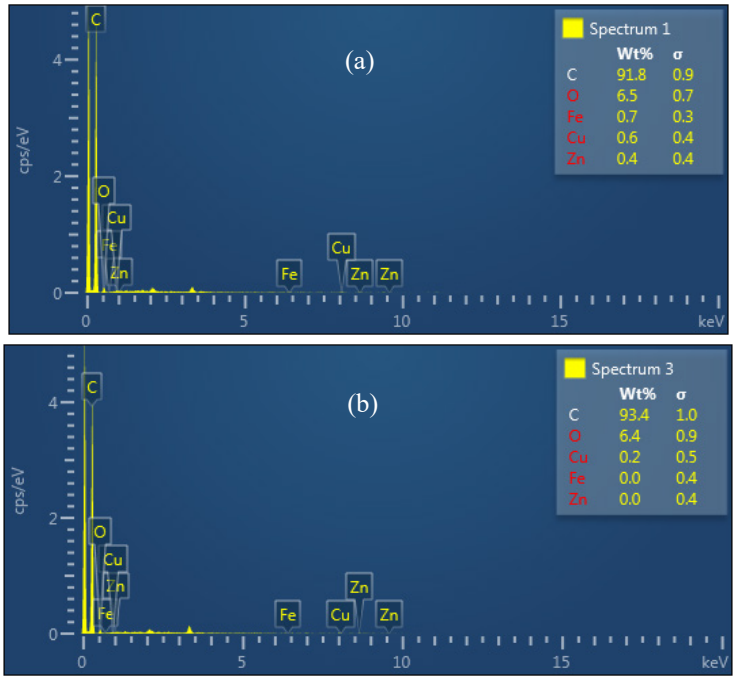

Figure 3 EDS results of the ACs made from (a) the oil extracted seed and (b) the non-oil extracted seed.

The SEM images of the AC with different views are illustrated in **Figure 4**. **Figure 4(a)** exhibited the external surface of the AC (side view). It was found that there were various sizes and shapes of small pores on the surface. **Figure 4(b)** showed the external surface from the top view of the AC. It revealed the well-developed pores on the external surfaces of the AC distributed uniformly. The result is in line with similar porous carbon materials [35,36].

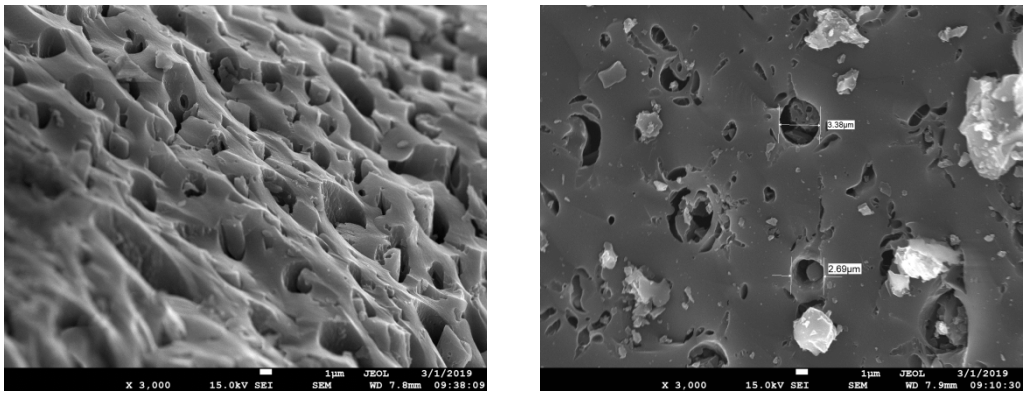

(a) (b)

Figure 4 SEM images of the AC with 3,000× magnitudes (a) side view and (b) top view.

Influence of contact time on the adsorption

The adsorption capacity of the AC rapidly increased in the first 20 min, gradually increased in the second stage (20 - 60 min) and leveled off after 60 min as shown in **Figure 5(a)**. The rapid increase in the first stage results from the fact that there are several available adsorptive sites on the external surface of the adsorbent, which is rid of the TT [37]. The dye molecules are able to occupy those surfaces easily. Then, the external surface is saturated. The dye particles diffuse into the interior of the adsorbent causing a slower increase of the dye uptake in the later stage [38]. Finally, the adsorbent becomes saturated with the TT molecules at the final stage (60 min) so the equilibrium time is 60 min.

Influence of initial pH on the adsorption

An increase in the initial pH caused an increase in TT dye uptake of the AC (**Figure 5(b)**), which was also found in literatures [39]. The characteristics of the adsorbent revealed the existence of anionic functional groups on the adsorbent surface. At the low pH, these anionic functional groups as mentioned earlier did not completely dissociate so they mostly stayed in the natural form. Physical adsorption dominated the adsorption process due to the high surface area of the adsorbent. Besides, the competition between the H^+ and the cations of TT dye molecules possibly caused the low dye uptake. At the high pH, the active functional groups were more dissociated and more negative charges were formed. Consequently, more dissociated functional groups resulted in the electrostatic interaction between the cationic TT dye particles and the anionic groups of the AC. In addition, the higher dye uptake resulted from the less competition between the dye and H^+. At the alkaline medium, the fraction of H^+ was low while that of OH^- was high. The highest dye uptake was 57.34 mg/g observed at the initial pH of 8.0.

The interactions between cationic species and the negatively charged AC surface are governed by 2 possible reactions. First, the reaction between the π electrons of the aromatic ring on the AC surface ($-C_\pi$) and H_2O produces $-C_\pi$ $-H_3O^+$ and OH^- as products ($-C_\pi + 2H_2O \rightarrow -C_\pi-H_3O^+ + OH^-$). The cation exchange between $-C_\pi-H_3O^+$ and TT^+ species subsequently occurs ($-C_\pi-H_3O^+ + TT^+ \rightarrow -C_\pi-TT + H_3O^+$) [40]. Second, the carboxylic groups appear on the AC surface as presented in the FTIR spectra so the surface acidity is an important factor. At the low pH, the adsorption of TT dye molecules onto the surface of the AC involves the reaction between polar functional groups (-COOH) and the cationic TT dye molecules ($R\text{-}COOH + TT^+ \rightarrow R\text{-}COOTT + H^+$). On the other hand, at the high pH, the polar functional groups are more dissociated from carboxylate group ($-COO^-$). The reaction between carboxylate groups and TT^+ molecules occurs ($R\text{-}COO^- + TT^+ \rightarrow R\text{-}COOTT$) [41]. Thus, the conversion of the second reaction is relatively high at the high pH solution.

Influence of initial dye concentration on the adsorption

Increasing the initial dye concentration increased the adsorption capacity of TT dye molecules on the AC (**Figure 5(c)**). The quantity of dye molecules adsorbed was a measurement of dye molecules loaded on the adsorbent surface or the quantity of dye molecules disappeared from the liquid solution. At the low dye concentration, the quantity of dye molecules adsorbed was low. It resulted from the fact that the small fraction of adsorptive sites on the AC was occupied by TT dye molecules and there were available adsorptive sites remained. When the initial concentration increased, more adsorptive sites were occupied by the TT dye molecules. The higher dye concentration in the bulk solution caused an increase in the driving forces (concentration difference between the adsorbent at the external surface and the internal surface). This resulted in a lower internal mass transfer resistance. Therefore, more adsorptive sites in the adsorbent interior were occupied [42,43]. The highest adsorption capacity was 28.75 mg/g observed at an initial dye concentration of 250 mg/L.

Influence of temperature on the adsorption

An increase in the adsorption capacity of the AC was caused by an increase in temperature (see **Figure 5(d)**). More dye molecules were adsorbed on the AC when the temperature was raised. This can be explained that the adsorption involves a chemical reaction and it is an endothermic process. When more energy is supplied by increasing the temperature, the equilibrium constant increases and the reaction is forward [44]. Additionally, an increase in temperature causes a physical change of the adsorbent and the dye molecules. The dye molecules can diffuse and occupy more adsorptive sites within the pore of the adsorbent. The highest adsorption capacity was 56.68 mg/g observed at a temperature of 60 °C.

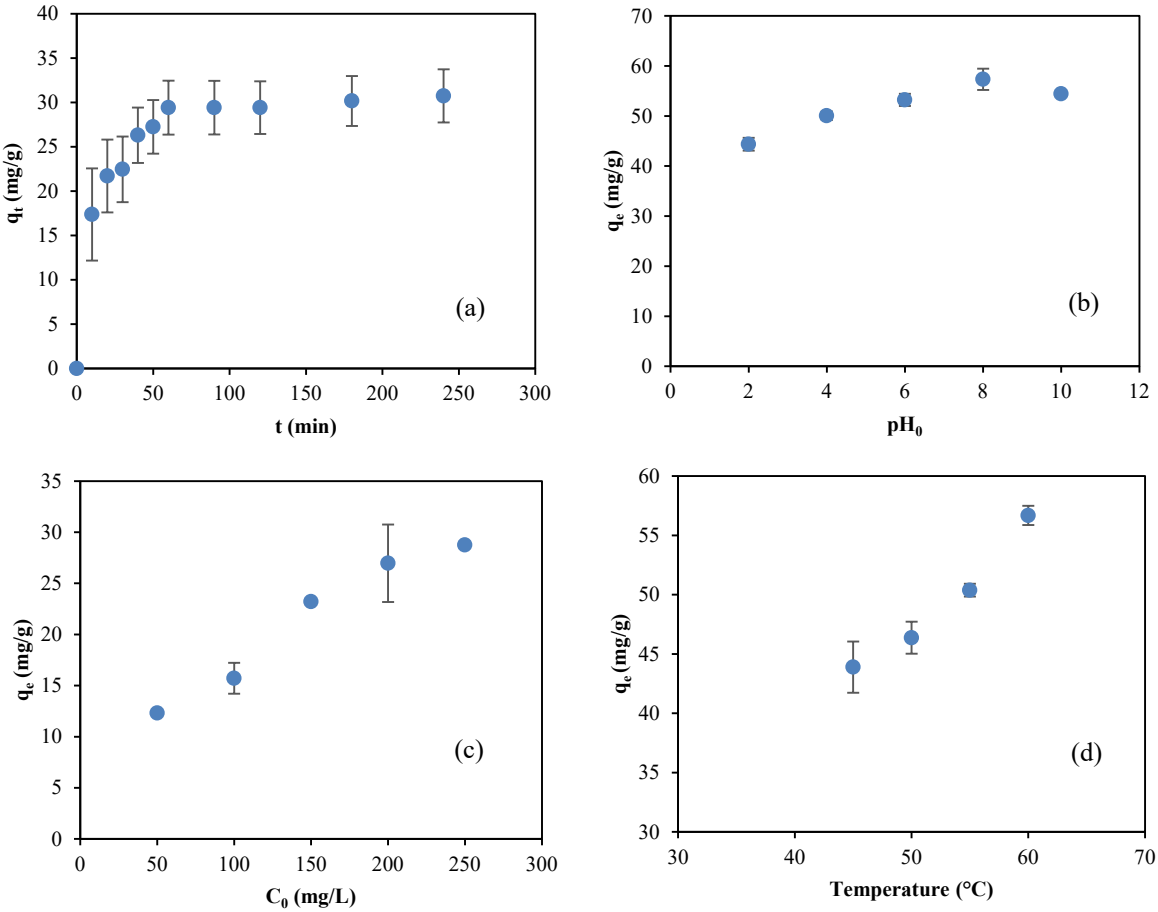

Figure 5 Adsorption capacity of TT molecules on the AC vs. various affecting factors (a) contact time, (b) initial pH, (c) initial concentration of dye solutions and (d) temperature.

Adsorption kinetic models

Adsorption mechanisms of the dye molecule on the adsorbent involve several steps. Initially, the dye molecule transports from the solution to the external stagnant film covering the adsorbent. The dye molecule then diffuses through the stagnant film. The interacting formation of the dye molecule on the external surface of the adsorbent is generated the next step. Later, the transport of the dye molecule occurs in the pore and it is finally adsorbed on the interior surface of the adsorbent. The rate limiting step which is the longest step is necessary to be identified. There are several kinetic models such as pseudo-first-order and pseudo-second-order reaction model and intraparticle kinetic models used as tools to determine the rate limiting step.

The pseudo-first-order reaction model was proposed by Lagegren [45]. This model is based on the rate equation of the homogeneous reaction to fit the kinetic data of the heterogeneous reaction and the 'pseudo' is addressed as a prefix. The linear form of this model can be expressed as following:

$$\ln(q_e - q_t) = \ln(q_t) - k_1 t \quad (1)$$

where q_e and q_t (mg/g) are the adsorption capacity of the dye molecules on the adsorbent at the equilibrium stage and at instantaneous time t, respectively. The parameters k_1 is the first order rate constant (1/min) and t is time (min). In case the chemical reaction is the rate-controlling step, the measured data agree with the pseudo-first-order reaction model. Normally, this model fits well to the first 30 min of the experimental data.

The pseudo-second-order reaction model was proposed by Ho and McKay [46]. This model uses the rate equation of the second-order homogeneous reaction to fit the kinetic data of the heterogeneous reaction and the 'pseudo' is addressed as a prefix. The linear form of this model can be given by:

$$\frac{t}{q_t} = \frac{1}{k_2 q_e^2} - \frac{t}{q_e} \quad (2)$$

where the parameters k_2 is the second order rate constant (g/(mg·min)). If the chemical reaction is the rate-controlling step, the measured data match the pseudo-second order reaction model.

The intra-particle diffusion model was developed by Weber and Morris [47]. This model is used to describe the transport property of metal ions from the solution to the interface, which can be expressed as following:

$$q_t = k_p t^{0.5} \quad (3)$$

where the parameters k_p is the intraparticle rate constant (mg/(g·min$^{0.5}$)) and C is the intercept of the straight line (mg/g) which gives information on the boundary layer thickness.

The parameters of the pseudo-first-order reaction, pseudo-second-order reaction, and intraparticle diffusion equations are summarized in **Table 3**. It was found that the experimental data followed the pseudo-second-order reaction equation because the R^2 value was the closest to 1.0. It exhibited that sharing of valence electrons between the TT dye molecules and the adsorptive surfaces of the adsorbent was the rate of limiting step. Therefore, this adsorption process involves a chemical reaction.

Table 3 Kinetic parameters for adsorption TT on the AC.

Kinetic adsorption model	Parameter	Value	Unit
Pseudo-first-order reaction model	$q_{e(exp)}$	30.74	mg/g
	k_1	0.05	1/min
	$q_{e,(cal)}$	24.27	mg/g
	R^2	0.962	-
Pseudo-second-order reaction model	k_2	0.009	g/(mg·min)
	$q_{e(cal)}$	28.17	mg/g
	R^2	0.975	-
Intraparticle diffusion model	k_p	3.820	mg/(g·min$^{0.5}$)
	C	2.311	mg/g
	R^2	0.951	-

Adsorption isotherm

Adsorption behavior is essential, which can be classified the patterns of the dye molecules binding on the adsorbent surface if they are monolayer or multilayer coverage. The adsorption isotherm is a relationship between equilibrium quantities of the dye molecules on the adsorbent versus the dye concentration at equilibrium. There are several isotherm models used to describe the adsorption behavior: Langmuir and Freundlich isotherm equations.

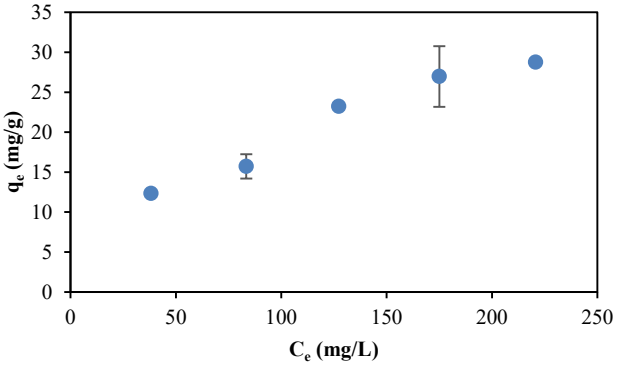

Figure 6 Adsorption isotherm of TT dye molecules on the AC.

Langmuir isotherm [48] is developed based on the assumption that the adsorbent surface is homogeneous or has a finite number of identical sites. The Langmuir isotherm equation in the linear form can be written as:

$$\frac{C_e}{q_e} = \frac{1}{k_L q_m} - \frac{C_e}{q_e} \quad (4)$$

where k_L is Langmuir constant (L/g) and q_m is the maximum monolayer adsorption capacity (mg/g). The important characteristics of the Langmuir isotherm is expressed by a separation factor or equilibrium parameter, "R_L". It is a dimensionless constant and defined as:

$$R_L = \frac{1}{1 + k_L C_0} \quad (5)$$

This parameter is used to indicate the type of isotherm. It is unfavorable ($R_L > 1$), linear ($R_L = 1$), favorable ($0 < R_L < 1$) or irreversible ($R_L = 0$).

Freundlich isotherm [49] is developed from the assumption that the adsorbent surface is heterogeneous or has various sites. The Freundlich isotherm equation in the linear form is written as:

$$\ln(q_e) = \ln(k_F) - \frac{1}{n}\ln(C_e) \quad (6)$$

where k_F and n are physical constants of Freundlich isotherm ($mg^{1-1/n} \cdot L^{1/n}/g$) The k_F and n indicate the adsorption capacity and adsorption intensity, respectively.

Table 4 Isotherm parameters for the adsorption of TT molecules on the AC.

Adsorption isotherm model	Parameter	Value	Unit
Langmuir isotherm	k_L	0.008	L/g
	q_m	44.25	mg/g
	R_L	0.04	-
	R^2	0.933	-
Freundlich isotherm	k_F	1.797	$(mg^{1-1/n} \cdot L^{1/n})/g$
	n	1.937	-
	R^2	0.960	-

The constants of Langmuir isotherm and Freundlich isotherm equations are summarized in **Table 4**. It was found that the experimental data fitted well to both Langmuir and Freundlich isotherm equations because their R^2 values were close to 1.0 as shown in **Figure 6**. It exhibited that the monolayer and multilayer coverages of TT dye molecules on the external surface of the adsorbent could occur.

Table 5 The maximum adsorption capacities of TT molecules by different sorbents calculated using the Langmuir model.

Sorbent	q_m, mg/g	Reference
AC	44.25	This study
Modified montmorillonite	95.36	[50]
Vesicularia dubyana moss	119.36	[51]
Hop leaf biomass	77.76	[52]
Rhytidiadelphus squarrosus	126.4	[53]
Fomitopsis carnea	21.98	[54]

The maximum adsorption capacity of this study has been in comparison with other organic and inorganic sorbents (**Table 5**). The Langmuir dye uptake of TT molecules onto the AC is mostly lower than other sorbents. However, the q_m in this work was obtained by the batch adsorption tests in different experimental conditions from other works such as contact time, pH solution, initial dye concentration, adsorbent particle size, and temperature, etc. The experimental design to determine the higher dye uptake should be further investigated.

Adsorption mechanisms

The possible interactions between the dye molecules and the adsorbent are depicted in **Figure 7**. The Symbol 1 stands for the adhesion of the dye molecule and the active site due to the van der Waals forces which can normally occur with any kind of molecules on the external surface of the adsorbent [55,56]. Symbol 2 represents the electrostatic attraction between the anionic functional groups of the AC and the cationic groups of the basic dye molecules [57,58]. This interaction is suggested due to an increase in the dye uptake with an increment of the initial pH. The increase in the initial pH causes more dissociation of the carboxyl and hydroxyl groups on the external surface of the adsorbent and strengthen the electrostatic interaction. Symbol 3 represents the interaction between the dye molecules and the internal surface (inside pore) of the adsorbent. This mechanism is expected due to a slow increase in the dye uptake with contact time in the second stage (see **Figure 7**). The slow increase results from the fact that the dye molecules diffuse into the pore of the adsorbent and then bind with the internal surface [59,60].

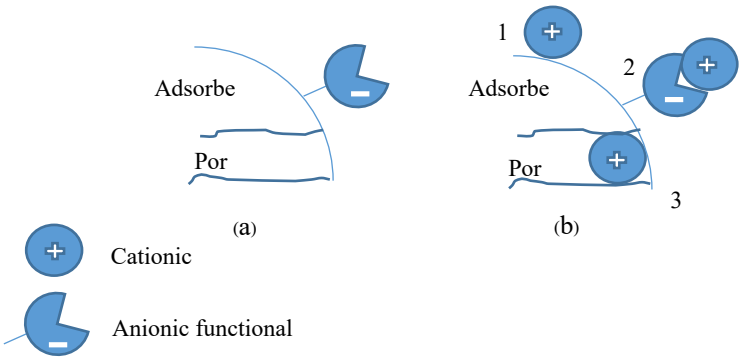

Figure 7 Adsorption mechanism scheme (a) adsorbent without the adsorbate and (b) adsorbent with dye molecules loaded.

Conclusions

The activated carbon (AC) prepared from the oil extracted *Elaeocarpus hygrophilus Kurz* seed is a microporous material. It has a high specific surface area and contains a fixed negative charge on the external surface, having high affinity to the cationic molecules. The adsorption capacity of the Thioflavin T (TT) dye, a cationic dye, increased with the increment of contact time, $pH_{0,}$ initial dye concentration and temperature. The highest adsorption capacity of TT dye molecules was suggested at a certain condition: contact time of 60 min, pH_0 of 8.0, C_0 of 250 mg/L, the temperature of 60 °C. The AC prepared from the oil extracted *Elaeocarpus hygrophilus Kurz* seed is a potential adsorbent for TT dye removal from effluent.

Acknowledgements

The authors would like to thank the Faculty of Engineering, Ubon Ratchathani University, Thailand for the partial financial support and be grateful to the National Research Council of Thailand in 2011 for another part of financial support.

References

[1] A Junsongduang, K Sirithip, A Inta, R Nachai, B Onputtha, W Tanming and H Balslev. Diversity and traditional knowledge of textile dyeing plants in northeastern Thailand. *Econ. Bot.* 2017; **71**, 241-55.

[2] C Xue, TY Lin, D Chang and Z Guo. Thioflavin T as an amyloid dye: Fibril quantification, optimal concentration and effect on aggregation. *Roy. Soc. Open Sci.* 2017; **4**, 160696.

[3] S Pai, MS Kini and R Selvaraj.A review on adsorptive removal of dyes from wastewater by hydroxyapatite nanocomposite. *Environ. Sci. Pollut. Res.* 2021; **28**, 11835-49.

[4] B Lellis, CZF Polonio, JA Pamphile and JC Poloio. Effects of textile dyes on health and the environment and bioremediation potential of living organisms. *Biotechnol. Sci. Innovat.* 2019; **3**, 275-90.

[5] KG Malmos, LMB Mejia, B Weber, J Buchner, MR Alvarado, H Naiki and D Otzen. ThT 101: A primer on the use of thioflavin T to investigate amyloid formation. *Amyloid* 2017; **24**, 1-16.

[6] J Damtab, P Nutaratat, W Boontham, N Srisuk, K Duangmal, H Yurimoto, Y Sakai, Y Muramatsu and Y Nakagawa. *Roseomonas elaeocarpi* sp. nov., isolated from olive (*Elaeocarpus hygrophilus* Kurz.) phyllosphere. *Int. J. Syst. Evol. Microbiol.* 2016; **66**, 474-80.

[7] J Suwanboriboon, W Meesiri and W Wongkokua. An application of spectrophotometer for ADMI color measurement. *J. Phys. Conf.* 2018; **1144**, 012064.

[8] D Bhatia, NR Sharma, J Singh and RS Kanwar. Biological methods for textile dye removal from wastewater: A review. *Crit. Rev. Environ. Sci. Tech.* 2017; **47**, 1836-76.

[9] V Katheresan, J Kansedo and SY Lau. Efficiency of various recent wastewater dye removal methods: A review. *J. Environ. Chem. Eng.* 2018; **6**, 4676-97.

[10] S Dawood and T Sen. Review on Dye removal from its aqueous solution into alternative cost effective and non-conventional adsorbents. *J. Chem. Proc. Eng.* 2014; **1**, 1-11.

[11] MAA Ghoutiand and AO Sweleh. Optimizing textile dye removal by activated carbon prepared from olive stones. *Environ. Tech. Innovat*. 2019; **16**, 100488.

[12] DS Duc, N Bin and TTH Trang. Adsorption of basic yellow 28 in aqueous solution by activated carbon. *Asian J. Chem.* 2013; **25**, 2173-76.

[13] AF Alkaim and MBH Alqaraguly. Adsorption of basic yellow dye from aqueous solutions by activated carbon derived from waste apricot stones: Equilibrium, and thermodynamic aspects. *Int. J. Chem. Sci.* 2013; **11**, 797-814.

[14] J Yener, T Kopac, G Dogu and T Dogu. Adsorption of basic yellow 28 from aqueous solutions with clinoptilolite and amberlite. *J. Colloid. Interface. Sci.* 2006; **294**, 255-64.

[15] R Aravindhan, JR Rao and BU Nair. Removal of basic yellow dye from aqueous solution by sorption on green alga *Caulerpa scalpelliformis*. *J. Hazard. Mater.* 2007; **142**, 68-76.

[16] F Boudrahem, FA Benissad and A Soualah. Removal of basic yellow dye from aqueous solutions by sorption onto reed as an adsorbent. *Desalination Water Treat*. 2015; **54**, 1727-34.

[17] M Ajbary, A Santos, VM Florez and L Esquivias. Removal of basic yellow cationic dye by an aqueous dispersion of Moroccan stevensite. *Appl. Clay Sci.* 2013; **80-81**, 46-51.

[18] S Saini, JK Katnoria and I Kaur. Surface modification of *Dendrocalamus strictus* charcoal powder using nitrilotriacetic acid as a chelating agent and its application for removal of copper(II) from aqueous solutions. *Separ. Sci. Tech.* 2021; **56**, 275-89.
[19] S Ho. Removal of dye by adsorption onto activated carbons: Review. *Eurasian J. Anal. Chem.* 2018, **13**, 332-8.
[20] A Martins and N Nunes. Adsorption of a textile dye on commercial activated carbon: A simple experiment to explore the role of surface chemistry and ionic strength. *J. Chem. Educ*. 2015; **92**, 143-7.
[21] Y Kuang, X Zhang and S Zhou. Adsorption of methylene blue in water onto activated carbon by surfactant modification. *Water* 2020; **12**, 587.
[22] D Sun, Z Zhang, M Wang and Y Wu. Adsorption of reactive dyes on activated carbon developed from *Enteromorpha prolifera*. *Am. J. Anal. Chem.* 2013; **4**, 17-26.
[23] S Saini, S Arora, Kirandeep, BP Singh, JK Katnoria and I Kaur. Nitrilotriacetic acid modified bamboo charcoal: An effective adsorbent for the removal of Cr(III) and Cr(VI) from aqueous solution. *J. Environ. Chem. Eng*. 2018; **6**, 2965-74.
[24] D Nayeri and SA Mousavi. Dye removal from water and wastewater by nanosized metal oxides-modified activated carbon: A review on recent researches. *J. Environ. Health. Sci. Eng.* 2020; **18**, 1671-89.
[25] U Gecgel, O Uner, G Gokara and Y Bayrak. Adsorption of cationic dyes on activated carbon obtained from waste *Elaeganus* stone. *Adsorption Sci. Tech.* 2016; **34**, 512-25.
[26] Y Lin, J Ma, W Liu, Z Li and K He. Efficient removal of dyes from dyeing wastewater by powder activated carbon charcoal/titanate nanotube nanocomposites: Adsorption and photoregeneration. *Environ. Sci. Pollut. Res.* 2019; **26**, 10263-73.
[27] S Yadav, A Asthana, R Chakraborty, B Jain, AK Singh, SAC Carabineiro and MABH Susan. Cationic dye removal using novel magnetic/activated charcoal/β-cyclodextrin/alginate polymer nanocomposite. *Nanomaterials* 2020; **10**, 170.
[28] M Ghasemi, S Mashhadi and J Azimi. Fe_3O_4/AC nanocomposite as a novel nano adsorbent for effective removal of cationic dye: Process optimization based on Taguchi design method, kinetics, equilibrium and thermodynamics. *J. Water Environ. Nanotechnology* 2018; **3**, 321-36.
[29] A Sencan and M Kilic. Investigation of the changes in surface area and FT-IR Spectra of activated carbons obrtained from hazelnut shells by physicochemical treatment methods. *J. Chem*. 2015; **2015**, 651651.
[30] D Cuhadaroglu and OA Uygun. Production and characterization of activated carbon from a bituminous coal by chemical activation. *Afr. J. Biotechnol.* 2008; **7**, 3703-10.
[31] E Pehlivan. Production and characterization of activated carbon from pomegranate pulp by phosphoric acid. *J. Turk. Chem. Soc. Chem.* 2018; **5**, 1-8.
[32] L Zhang, LY Tu, Y Liang, Q Chen, ZS Li, CH Li, ZH Wang and W Li. Coconut-based activated carbon fibers for efficient adsorption of various organic dyes. *RSC Adv*. 2018; **8**, 42280-91.
[33] NM Zawawi, F Hamzah, M Sarif, SFA Manaf and A Idris. Characterization of activated carbon using chemical activated carbon via microwave ultrasonic system. *Malaysian J. Anal. Sci.* 2017; **21**, 159-65.
[34] A. Allwar. Preparation and characteristics of activated carbon from oil palm shell for removal of iron and copper from patchouli oil. *Int. J. Appl. Chem.* 2016; **12**, 183-92.
[35] PO Bedolla, G Feldbauer, M Wolloch, SJ Eder, N Dorr, P Mohn, J Redinger and Andras V. Effects of van der Waals interactions in adsorption of isooctane and ethanol on Fe(100) surfaces. *J. Phys. Chem. C* 2014; **118**, 17608-15.
[36] S Lim, JH Kim, H Park, C Kwak, J Yang, J Kim, SY Ryu and J Lee. Role of electrostatic interactions in the adsorption of dye molecules by Ti_3C_2-MXenes. *RSC Adv*. 2021; **11**, 6201-11.
[37] S Moosavi, CW Lai, S Gan, G Zamiri, OA Pivehzhani and MR Johan. Application of efficient magnetic particles and activated carbon for dye removal from wastewater. *ACS Omega* 2020; **5**, 20684-97.
[38] NUM Nizam, MM Hanafiah, E Mahmoudi, AA Halilm and AW Mohammad. The removal of anionic and cationic dyes from an aqueous solution using biomass-based activated carbon. *Sci. Rep.* 2021; **11**, 8623.
[39] Y Zhou, Z Wang, A Hursthouse and B Ren. Gemini surfactant-modified activated carbon for remediation of hexavalent chromium from water. *Water* 2018; **10**, 91.

[40] EA Deliyanni, GZ Kyzas, KS Triantafyllidis and KA Matis. Activated carbons for the removal of heavy metal ions: a systematic review of recent literature focused on lead and arsenic ions. *Open Chem*. 2015; **13**, 699-708.
[41] MJ Baniamerian, SE Moradi, A Noori and H Salahi. The effect of surface modification on heavy metal ion removal from water by carbon nanoporous adsorbent. *Appl. Surf. Sci.* 2009; **256**, 1347-54.
[42] J Shu, S Cheng, H Xia, L Zhang, J Peng, C Li and S Zhang. Copper loaded on activated carbon as an efficient adsorbent for removal of methylene blue. *RSC Adv*. 2017; **7**, 14395-405.
[43] T Phothitontimongkol, N Kumaiard and Y Tantipalakul. Activated carbon from tamarind wood supported TiO_2 for methylene blue dye removal in wastewater by photocatalytic process. *Burapha Sci. J.* 2016; **21**, 73-91.
[44] NTA Ghani, GAE Chaghaby, ESA Rawash and EC Lima. Adsorption of coomassie brilliant blue R-250 dye onto novel activated carbon prepared from *Nigella Saiva* L. waste: Equilibrium, kinetics and thermodynamics running title: Adsorption of brilliant blue dye onto *Nigella Sativa* L. waste activated carbon. *J. Chilean Chem. Soc*. 2017; **62**, 3505-11.
[45] S Lagegren. About the theory of so-called adsorption of soluble substances. *Kungliga Svenska Vetenskapsakademiens Handlingar* 1989; **24**, 1-39.
[46] YS Ho and G Mckay.Sorption of dye from aqueous solution by peat. *Chem. Eng. J*. 1998; **70**, 115-24.
[47] WJ Weber Jr and JC Morris. Kinetics of adsorption on carbon from solution. *J. Sanitary Eng. Div.* 1963; **18**, 31-42.
[48] I Langmuir. The adsorption of gases on plane surfaces of glass, mica and platinum. *J. Am. Chem. Soc.* 1918; **40**, 1361-8.
[49] MSN Tabbiruka and L Lungani. Removal of dyes from wastewaters through adsorption using HCl activated coal. *J. Mater. Chem*. 2018; **8**, 23-30.
[50] WS Shin. Competitive sorption of anionic and cationic dyes onto cetylpyridinium-modified montmorillonite. *J. Environ. Sci. Health* 2008; **43**, 1459-70.
[51] M Pipiska, M Valica, D Partelova, M Hornik, J Lesny and S Hosin. Removal of synthetic dyes by dried biomass of freshwater moss vesicularia dubyana: A batch biosorption study. *Environ.* 2018; **5**, 10.
[52] D Partelova, A Sunovska, J Maresova, M Hornik, M Pipska and S Hostin. Removal of contaminants from aqueous soluitons using Hop (*Humulus lupulus L.*) agricultural by-products. *Nova Biotechnol. Et Chim*. 2015; **14**, 212-27.
[53] L Remenrova, M Pipiska, M Hornik and J Augustin. Sorption of cationic dyes from aqueous solutions by moss Rhytidiadelphus squarrosus: Kinetics and equilibrium studies. *Nova Biotechnol*. 2009; **9**, 53-61.
[54] N Maurya and AK Mittal. Biosorptive uptake of catinic dyes from aqueous phase using immobilised dead macro fungal biomass. *Int. J. Environ. Tech. Manag.* 2011; **14**, 282-93.
[55] S Sivaprakash, PS Kumar and SK Krishan. Adsorption study of various dyes on activated carbon Fe_3O_4 Magnetic nanocomposite. *Int. J. Appl. Chem*. 2017; **13**, 255-66.
[56] OS Bello, KA Adegoke, OO Sarumi and OS Lameed. Functional locust bean pod (*Parkia biglbosa*) activated carbon for rhodamine B dye removal. *Heliyon* 2019; **5**, e02323.
[57] ML Firdaus, N Krisnanto, W Alwi, R Muhammad and MA Serunting. Adsorption of textile dye by activated carbon made from rice straw and palm oil midrib. *Aceh. Int. J. Sci. Tech*. 2017; **6**, 1-7.
[58] Y Cai, L Liu, H Tian, Z Yang and X Luo. Adsorption and desorption performance and mechanism of tetracycline hydrochloride by activated carbon-based adsorbents derived from sugar cane baggase activated with $ZnCl_2$. *Mol*. 2019; **24**, 4534.
[59] K Ebisike, AE Okoronkwo and KK Alaneme. Nickel sorption onto chitosan-silica hybrid aerogel from aqueous solution. *Walailak J. Sci. Tech.* 2021; **18**, 9454.
[60] AH Alamin and L Kaewsichan. Adsorption of Pb(II) ions from aqueous solution in fixed-bed column by mixture of clay plus bamboo biochar. *Walailak J. Sci. Tech.* 2016; **13**, 949-63.